Human Molecular Genetics, 1999, Vol. 8, No. 2 **195–204**

ARTICLE

Xist RNA exhibits a banded localization on the inactive X chromosome and is excluded from autosomal material *in cis*

Sarah M. Duthie[1], Tatyana B. Nesterova[1,2], Emma J. Formstone[1], Ann M. Keohane[3], Bryan M. Turner[3], Suren M. Zakian[2] and Neil Brockdorff[1,*]

[1]X Inactivation Group, MRC Clinical Sciences Centre, Imperial College School of Medicine, Hammersmith Hospital, DuCane Road, London W12 0NN, UK, [2]Institute of Cytology and Genetics, Russian Academy of Sciences, Siberian Department, Novosibirsk 630090, Russia and [3]Chromatin and Gene Expression Group, University of Birmingham Medical School, Edgbaston, Birmingham B15 2TT, UK

Received October 27, 1998; Revised and Accepted November 7, 1998

The propagation of X chromosome inactivation is thought to be mediated by the *cis*-limited spreading of the non-protein coding *Xist* transcript. In this report we have investigated the localization of *Xist* RNA on rodent metaphase chromosomes. We show that *Xist* RNA exhibits a banded pattern on the inactive X and is excluded from regions of constitutive heterochromatin. The banding pattern suggests a preferential association with gene-rich, G-light regions. Analysis of X:autosome rearrangements revealed that restricted propagation of X inactivation into *cis*-linked autosomal material is reflected by a corresponding limited spread of *Xist* RNA. We discuss these results in the context of models for the function of *Xist* RNA in the propagation of X inactivation.

INTRODUCTION

X chromosome inactivation (X inactivation) is the mechanism by which the gene dosage in XX female mammals is equalized relative to XY males (reviewed in ref. 1). Early in embryogenesis, one X chromosome is chosen at random to be inactivated, followed by the bi-directional spread of silencing *in cis* from the X inactivation centre (Xic) (reviewed in ref. 2). The inactive state is then stably maintained during the cell cycle and in subsequent cell divisions. Following inactivation, the silenced X chromosome is visible as the Barr body (3,4), a heterochromatic structure located near the nuclear envelope. Other features that distinguish the inactive X (Xi) from its active homologue (Xa) include late replication, underacetylation of histones H3 and H4 (5–7) and hypermethylation of CpG islands (8).

The inactivation of coat colour markers in X:autosome (X:A) rearrangements provided the initial basis for defining a *cis* requirement for the Xic in the propagation of X inactivation (reviewed in ref. 9). Inactivation spreads variably and reversibly into autosomes and, importantly, autosomal genes closer to the X:A break point are more readily silenced than those further away. This attenuated spreading effect was initially described as an example of position effect variegation (PEV) (10). The resistance of autosomal material to X-inactivation led Riggs to propose that specific elements, or 'way stations', distributed along the X facilitate the spreading signal (8). These elements should be either less frequent, or absent, on autosomes or on regions of the X that are known to escape inactivation, such as the pseudo-autosomal region.

Identification of the human and mouse *XIST*/*Xist* genes which map to the *XIC*/*Xic* region (11–13) provided a major breakthrough in the molecular analysis of X inactivation. The *Xist* gene is expressed exclusively from the Xi in somatic cells and produces a 15 kb RNA that has no significant open reading frame and is retained in the nucleus. Recently it has been shown that the presence of the *Xist* gene *in cis* is both necessary and sufficient for X inactivation to occur (14–18).

The application of RNA fluorescence *in situ* hybridization (FISH) techniques has provided important insights into the involvement of the *Xist* gene in the inactivation process. In 1992, Brown *et al*. (19) showed that the *XIST* transcript 'paints' the Barr body in interphase nuclei. Clemson *et al*. (20) confirmed this finding and proposed that the *XIST* transcript acts as a link between Xi chromatin and the nuclear matrix. The authors also demonstrated that human *XIST* RNA dissociates from the X chromosome as cells enter mitosis and appears to be retranscribed in daughter cells from early G_1. In contrast, studies on murine cells indicate that the association of *Xist* RNA with Xi continues at least until metaphase (16). Recent analyses of ectopic *Xist* transgenes have reported *cis* accumulation of RNA on autosomal

*To whom correspondence should be addressed. Tel: +44 181 383 8298; Fax: +44 181 383 8303; Email: nbrockdo@hgmp.mrc.ac.uk

material (15,16,18). Most notably, a multicopy 450 kb *Xist* transgene located on chromosome 12 was shown to inactivate autosomal genes located at some distance from the YAC integration site. *Xist* RNA was reported to cover the entire autosome, with no skipped regions except for the centromere (15,16).

To further our understanding of the X inactivation spreading mechanism, we have investigated the localization of *Xist* RNA on rodent X chromosomes at metaphase. Taking advantage of the unique morphology of the X chromosome in certain species of the common vole, *Microtus arvalis*, we showed that *Xist* RNA does not bind indiscriminately to X chromatin *in cis* but exhibits a specific banded localization that resembles R banding (G-light bands). Banding was also observed on Xi in mouse and rat cell lines. The vole X chromosomes carry giant blocks of constitutive heterochromatin comprising up to 50% of the chromosome. We demonstrated that *Xist* RNA is completely excluded from these regions. We went on to analyse *Xist* RNA localization on mouse X:A rearrangements. Intriguingly, our results revealed that *Xist* RNA exhibits little or no spread into *cis*-linked autosomal material. We discuss these results in the light of models for the spread of X chromosome inactivation.

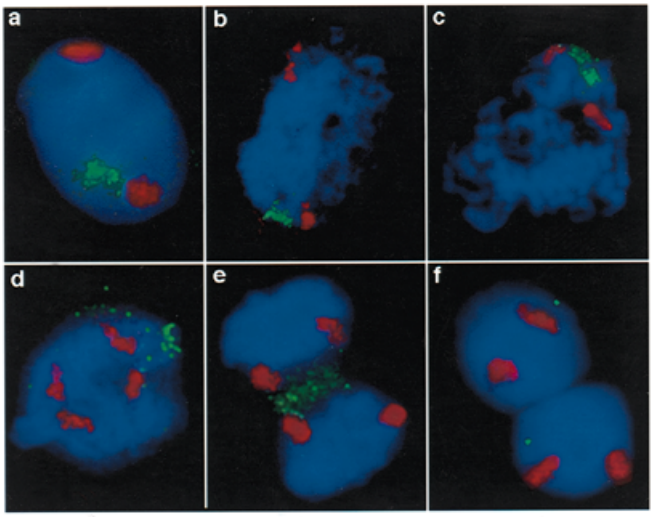

Figure 1. Progression of *Xist* RNA localization through the cell cycle in the vole *M.transcaspicus*. DNA/RNA FISH analysis of vole cells showing *Xist* RNA detected with FITC (green) and heterochromatin block repeat DNA detected with TR (red) illustrated on cells at (**a**) interphase, (**b**) prophase, (**c**) metaphase, (**d**) anaphase, (**e**) telophase and (**f**) daughter cells in early G_1. DNA was counterstained with DAPI.

RESULTS

Xist RNA localization on rodent metaphase chromosomes

RNA FISH was used to examine *Xist* RNA localization in several rodent primary fibroblast cultures, including the common voles, *Microtus transcaspicus* and *M.rossiaemeridionalis*, mouse and rat. Figure 1 illustrates results obtained for fibroblasts derived from the common vole species *M.transcaspicus* (21–24). *Xist* RNA appears as a large domain of discrete, punctate dots on only one of the two X chromosomes in the interphase nucleus (Fig. 1a) as described previously in human (20) and mouse (15) cells. In vole fibroblasts the X chromosome was identified by DNA FISH using the repeat MS3, a probe specific for a large X-linked constitutive heterochromatin block (25; see below).

We followed *Xist* localization through the cell cycle in voles from interphase to daughter cells (Fig. 1a–f). *Xist* RNA remains associated with the inactive X chromosome until anaphase, contrasting with human *XIST* which dissociates from Xi at prophase (20). At telophase the RNA dissociates from Xi and appears as dispersed clusters concentrated in the plane of cleavage (Fig. 1e). Daughter cells in early G_1 exhibit small punctate foci of signal, suggesting that *Xist* RNA is rapidly resynthesized following mitosis (Fig. 1f), as was reported for human cell lines (20). Similar results were also observed in other rodent species, including the common vole *M.rossiaemeridionalis*, mouse and rat (data not shown).

Association of the *Xist* transcript with the rodent Xi at metaphase provided a good opportunity to examine the relationship between *Xist* RNA and X chromatin. A critical feature of these experiments was the use of minimally disruptive conditions and formaldehyde crosslinking to fix the RNA (see Materials and Methods). We found that cytogenetic fix (methanol/acetic acid) did not adequately preserve the integrity of the RNA signal. Intriguingly, we discovered that *Xist* RNA is not distributed linearly along the length of the X chromosome, but rather appears as a series of distinct bands. The banded pattern occurs as paired foci along the length of the chromosome, suggesting association with equivalent sites on the sister chromatids. Examples of this banding are illustrated for the vole *M.transcaspicus* (Fig. 2a) and mouse (Fig. 2b). The majority of metaphase X chromosomes (60–70%) have a banded appearance over the whole of the Xi in all rodent cell lines examined. The remainder exhibited either partial coverage of the X chromosome or absence of RNA signal, possibly due to sample disruption or chromosome loss during preparation.

Interestingly, we noted that *Xist* transcript is excluded from the giant block of constitutive heterochromatin on vole X chromosomes. This is illustrated in Figure 1 for *M.transcaspicus* and in Figure 2d and e for *M.rossiaemeridionalis*. In mouse, *Xist* RNA does not associate with centromeric heterochromatin on the X chromosome, shown by double labelling for *Xist* RNA and a minor satellite DNA repeat (Fig. 2c).

The absence of *Xist* from regions of constitutive heterochromatin suggested that the banded localization of *Xist* RNA along the rest of the chromosome could reflect exclusion of the transcript from late replicating, Giemsa-positive (G-dark) chromosome bands. We examined the banded *Xist* RNA signal in the various rodent species and found a remarkably good correlation between the position and frequency of G-dark bands and apparent gaps in the *Xist* RNA signal. This is illustrated in Figure 2d and e for the *M.rossiaemeridionalis* X chromosome. Gaps in *Xist* RNA signal correlate with the position of the centromere at Xq1.1–1.4 and the large G-dark band at Xq1.8–1.12. Smaller gaps coincide with four G-dark bands at Xq2.4–2.5, Xq2.9, Xq2.12 and Xq2.18. The banding pattern is consistent and reproducible on X chromosomes from a number of different metaphases in this species.

Analysis of X:autosome rearrangements: Cattanach's translocation (Is1Ct)

The banding pattern observed on rodent metaphase chromosomes suggests that *Xist* RNA does not propagate indiscriminately along the X chromosome *in cis*. To investigate this further we examined

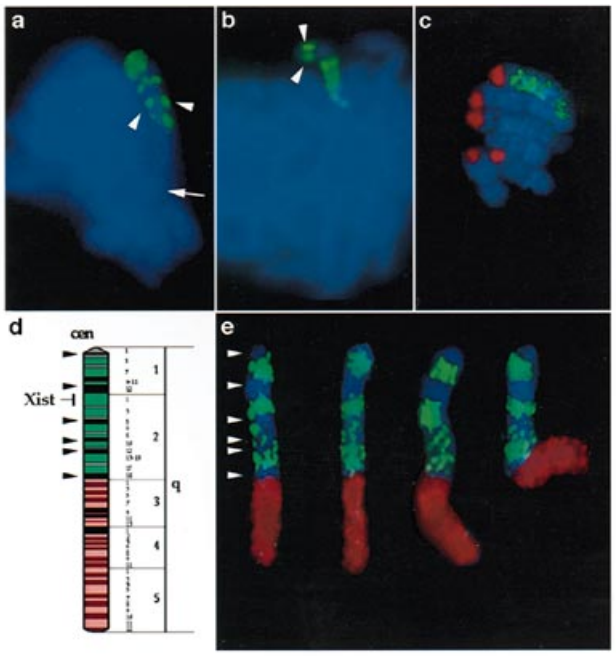

Figure 2. Localization of *Xist* RNA to discrete regions on rodent metaphase X chromosomes. (**a**) Illustration of banded localization of *Xist* RNA (FITC, green) to *M.transcaspicus* metaphase X chromosome. Arrowheads highlight paired foci on sister chromatids, arrow indicates position of centromere. (**b**) Banded localization of *Xist* RNA (FITC, green) to metaphase X chromosome of mouse XX fibroblast cell (cell line SD1) showing paired foci, indicated by arrowheads. (**c**) *Xist* RNA signal does not co-localize with centromeric heterochromatin indicated by DNA/RNA FISH for *Xist* RNA (FITC, green) and centromeric heterochromatin DNA (TR, red) on metaphase X chromosomes of mouse XX fibroblasts (cell line Is1Ct). (**d** and **e**) Ideogram and DNA/RNA FISH of the *M.rossiaemeridionalis* X chromosome. On the ideogram the giant heterochromatic block is illustrated in red and the remainder of the chromosome in green. Filled arrowheads mark G-dark bands in (d) which correlate with the location of gaps in *Xist* RNA signal indicated by arrowheads in (e). FISH was for *Xist* RNA (FITC, green) and heterochromatin block DNA (TR, red). Cells were counterstained for DNA (DAPI, blue).

Xist RNA localization in mice carrying X:A rearrangements. Initially we examined the X:A rearrangement Is(In7;X)1Ct (abbreviated to Is1Ct), an insertion of a region of chromosome 7 into the X chromosome (Fig. 3a). Primary fibroblast cultures were established from T(X;16)16H/Is1Ct female double heterozygotes. In these animals, the Is1Ct X chromosome is always the inactive X. DNA FISH analysis with mouse chromosome-specific paints confirmed the X chromosome constitution of these cell lines (data not shown).

Hypoacetylation of histone H4 is associated with transcriptional repression (5,26,27) and was chosen, therefore, as an indirect cytogenetic marker for the spread of the inactivating signal. The mouse Xi is generally pale staining with the exception of the pseudo-autosomal region (PAR), a region in band A2 near the centromere, and another in band F1 (5). The Is1Ct Xi has an additional broad acetylated region close to the PAR (Fig. 3b and c). Simultaneous detection of acetylated histone H4 with an X chromosome paint or the gene-specific markers *D7HD12* and *SnrpN* (Fig. 3a) confirmed that this broad band corresponds to the chromosome 7 insertion (Fig. 3d). The insertion is hyperacetylated on the majority (93%) of Is1Ct X chromosomes. In a minority of chromosomes (5%), the region of hyperacetylation on the Is1Ct X appeared to extend from the inserted region to the telomere with no gap. This may be due to chromosome condensation obscuring the hypoacetylated Xi material between the insertion and the PAR. Alternatively, the autosomal insertion may have blocked spread of the inactivating signal into the distal portion of Xi. In an even smaller number of spreads (2%), the Is1Ct X was completely hypoacetylated. This is possibly due to technical factors such as the quality of chromosome spreads, which was variable within individual slides, or the silencing mechanism may have spread efficiently through the insertion. These results are summarized in Figure 3h.

To determine whether *Xist* RNA localization corresponded to the regions of observed hypoacetylation on the Is1Ct Xi, DNA/RNA FISH was used to visualize the *D7HD12* and *SnrpN* loci together with *Xist* RNA (Fig. 3e–g). Strikingly, little or no spread of *Xist* RNA signal into the inserted chromosome 7 material was observed on the majority (68%) of Is1Ct X chromosomes (Fig. 3e). In 28% of chromosomes, the *Xist* RNA signal co-localized with one or both of the DNA probe signals, suggesting that the RNA had spread just inside the boundaries of the insertion, at least as far as the *SnrpN* and/or *D7HD12* loci (Fig. 3f). In a minority (4%) of metaphases, we observed faint clusters of *Xist* signal scattered along the entire inserted region (Fig. 3g). It is possible that these faint clusters occur in the insertion on all Is1Ct X chromosomes, but are difficult to resolve in conjunction with the strong *Xist* signal associated with Xi chromatin. Thus *Xist* RNA appears to associate more efficiently with X chromatin than with the *cis*-linked autosomal insertion in Cattanach's translocation, in agreement with the histone H4 data described above. The results are summarized in Figure 3i.

Analysis of X:autosome rearrangements: balanced reciprocal translocation T(X;4)37H

X inactivation and *Xist* localization was also examined in primary fibroblasts derived from T(X;4)37H (abbreviated to T37H) female mice. T37H is a balanced, reciprocal translocation with a short X^4 product and a long 4^X product that includes the Xic (Fig. 4a). We observed inactivation of either the 4^X product or the normal X chromosome, consistent with the fact that X inactivation is essentially random in adult T37H animals (28). Metaphases in which the readily identifiable 4^X product was inactive were analysed in detail. Spread of inactivation was assessed using an X chromosome paint or gene-specific probes for the *diabetes* (*db*) and *brown* (*b*) loci on chromosome 4 (Fig. 4a). Classical genetic studies on T37H indicate that inactivation can spread as far as *b* (10).

Cytogenetic analysis of histone H4 acetylation indicates that there is only very limited spread of inactivation into the autosomal material. Approximately 90% of 4^X chromosomes were pale staining on the X portion (except for the PAR region), with a sharp boundary at the translocation break point, as indicated by the X chromosome paint or gene-specific probes (Fig. 4a–d). In 3% of chromosomes, the hypoacetylated region appeared to extend as far as the *db* locus. There were no examples in which the entire 4^X chromosome was hypoacetylated. On the remaining metaphases (7%) we observed an isolated region of hypoacetylation between the gene-specific loci on the 4^X marker chromosome (data not shown). The level of resolution afforded by this approach means that the significance of the latter observation is not clear (see Discussion). The results are summarized in Figure 4h.

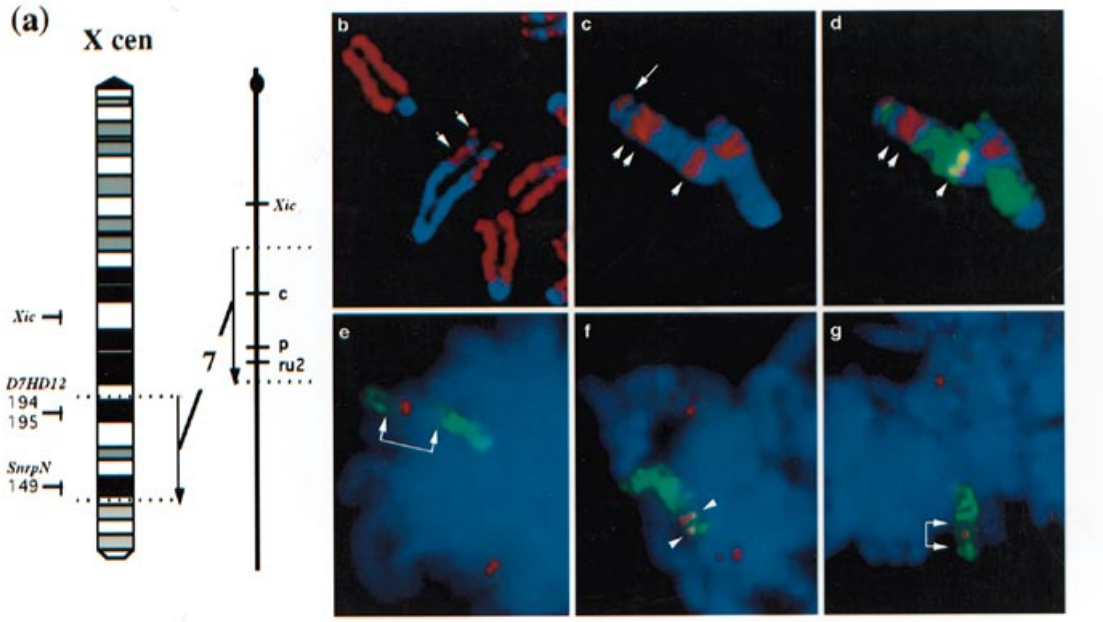

(h)

Is1Ct X H4 Ab + BACs	% of metaphases (n = 179)
7	93
7	5
7	2

(i)

Is1Ct X *Xist* RNA + BACs	% of metaphases (n = 119)
7	68
7	28
7	4

Figure 3. X inactivation and *Xist* localization in X:A rearrangement Is1Ct. (**a**) Ideogram and genetic map of the Is1Ct X chromosome indicating break points and position of loci discussed in the text. (**b**) Localization of acetylated histone H4 on an Is1Ct X chromosome using antibody 232 (TR, red); hyperacetylated regions are marked by arrows. (**c**) Two Is1Ct X chromosomes showing acetylated histone H4 banding in more detail; hyperacetylated band A2 (arrow), broad band of hyperacetylation (double arrow) and PAR (tailed arrow). (**d**) Double labelling of the same Is1Ct X chromosomes in (c) with acetylated H4 antibody (TR, red) and X chromosome paint (FITC, green). The single arrow indicates overlap of X paint and H4 hyperacetylated band A2 (yellow signal), double arrow shows no overlap of X paint and broad H4 hyperacetylated region. (**e**–**g**) Examples of DNA/RNA FISH on Is1Ct X metaphases showing *Xist* RNA (FITC, green) and *D7Hd12/SnrpN* loci (TR, red). Isolated red signals represent *D7Hd12/SnrpN* autosomal loci. (e) No spread of *Xist* RNA into autosome; large gap in RNA signal is marked by arrows. (f) Restricted spread of *Xist* RNA as far as *D7Hd12/SnrpN* loci; overlap of *Xist* RNA and DNA loci indicated by yellow signal and marked by arrows. (g) Weak spread of *Xist* RNA throughout insertion, marked by arrows. (**h**) Summary of histone H4 acetylation patterns on Is1Ct X chromosome. Red shading represents hyperacetylated regions; *D7Hd12* and *Snrp N* loci are indicated by green circles. (**i**) Summary of *Xist* RNA localization analysis: green shading represents regions covered with *Xist* RNA; light shading indicates weak *Xist* signal over the inserted material. The DNA loci are represented by red circles.

Consistent with the acetylation data, we observed limited spreading of *Xist* RNA into chromosome 4 material. In 48% of metaphases, *Xist* RNA localizes to the distal half of 4^X with a sharp boundary in the middle of the chromosome. Interestingly, we noted that in most cases there was an isolated focus of *Xist* within the region bounded by the chromosome 4 probes (Fig. 4e). In 44% of metaphases the *Xist* RNA signal extended as far as the *db* locus, but not beyond it (Fig. 4f). In the remaining 8% of spreads, the RNA had spread through both the *db* and the *b* loci on chromosome 4, but the signal became progressively weaker and never reached the chromosome 4 centromere (Fig. 4g). The results are summarized in Figure 4i. Thus, as with Is1Ct, the analysis of the T37H translocation demonstrates restricted spread of *Xist* RNA into autosomal material *in cis*.

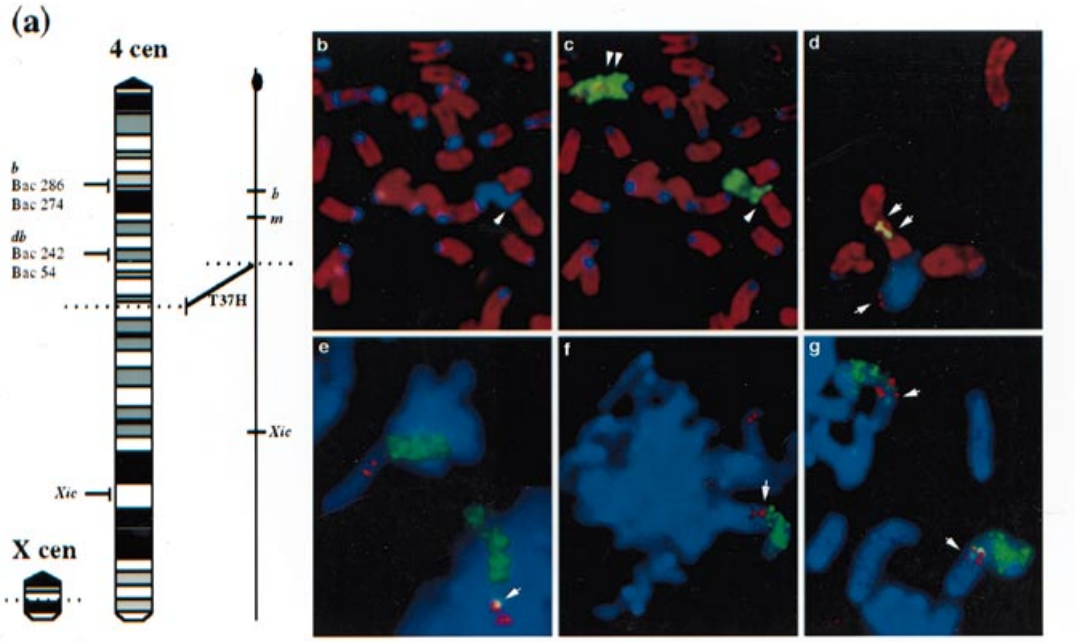

(h)

T37H 4^x H4 Ab + BACs	% of metaphases (n = 86)
4	90
4	3
4	7

(i)

T37H 4^x *Xist* RNA + BACs	% of metaphases (n = 52)
4	48
4	44
4	8

Figure 4. X inactivation and *Xist* localization in balanced translocation T37H. (**a**) Ideogram of X^4 and 4^X products in T37H and genetic map of 4^X product indicating location of break points and loci discussed in the text. (**b**) Localization of acetylated histone H4 on inactive T37H 4^X chromosome using antibody 232 (TR, red); the arrow marks the boundary between hyper- and hypoacetylated chromatin. (**c**) Double labelling of the same spread as in (b) with acetylated H4 antibody (TR, red) and X chromosome paint (FITC, green); the arrow marks the translocation break point on inactive 4^X chromosome. Only the X portion of the chromosome is hypoacetylated. The normal active X chromosome is hyperacetylated (double arrow). (**d**) Double labelling of inactive 4^X chromosome with acetylated H4 antibody (TR, red) and probes for the *b* and *db* loci (FITC, yellow signals due to overlap with antibody) indicated by arrows. The hyperacetylated PAR is marked by a single arrow. (**e**–**g**) Examples of DNA/RNA FISH on inactive 4^X metaphase chromosomes showing *Xist* RNA (FITC, green) and *b*/*db* loci (TR, red). The isolated red signal represents autosomal *b*/*db* loci. (e) Two 4^X chromosomes showing sharp boundary of *Xist* RNA at some distance from autosomal loci. Isolated focus of Xist between *db* and *b* indicated by arrow. (f) Restricted spread of *Xist* RNA as far as *db*/*b* loci, indicated by arrow. (g) Weak spreading of *Xist* RNA as far as the *b* locus, indicated by arrow. (**h**) Summary of histone H4 acetylation patterns on inactive 4^X chromosome. Red shading represents hyperacetylated regions; the *db* and *b* loci are represented by green circles. (**i**) Summary of analysis of *Xist* RNA localization. Green shading represents regions covered with *Xist* RNA, the isolated focus of *Xist* RNA between the *db* and *b* loci is represented by green circles and the DNA loci are represented by red circles.

DISCUSSION

In this report we have used FISH techniques to study the association of rodent *Xist* RNA with the inactive X chromosome at metaphase. Our results show that the *Xist* transcript specifically localizes to non-heterochromatin domains on the inactive X, in a discrete banded pattern. We suggest that gaps in the *Xist* RNA banding pattern correlate with the location of late replicating, G-dark bands. In addition, using the X:A rearrangements Is1Ct and T37H we demonstrate that *Xist* RNA associates more efficiently with X chromatin than with *cis*-linked autosomal material.

Localization of *Xist* RNA to the rodent metaphase Xi

The visualization of rodent *Xist* RNA at metaphase, using RNA FISH under minimally disruptive conditions, afforded the opportunity to relate *Xist* localization to known features of metaphase chromosome structure. Exclusion of *Xist* RNA from the giant blocks of constitutive heterochromatin on the vole X chromosomes provided a clear demonstration that the RNA shows a restricted localization pattern and is not uniformly distributed over the X chromosome. Analysis of the large vole X chromosomes also revealed the banded pattern of *Xist* localization, which appears to correspond to X chromosome G-banding. Further investigations are needed to confirm this relationship. It would also be interesting to investigate the relationship between genes that are known to escape inactivation and the *Xist* banding pattern. Banding was found to be highly dependent on fixation conditions. Cytogenetic fix (methanol/acetic acid) completely disrupted the pattern and some disruption also occurred following DNA denaturation in double labelling experiments. These observations may explain why banding has not been detected in previous studies on metaphase chromosomes (16,29).

It is plausible that the gaps in the *Xist* signal at metaphase result from premature dissociation of the RNA during sample preparation. Exclusion of *Xist* RNA from heterochromatin blocks in voles was evident, however both at interphase and metaphase and we therefore consider it likely that gaps observed in the *Xist* signal at metaphase accurately reflect the localization of *Xist* on Xi at interphase. We cannot rule out that there is a low level of *Xist* RNA associated with G-dark bands and constitutive heterochromatin, undetectable by FISH. Preferential association with G-light bands correlates with high gene density in these regions. By extension, G-dark bands and constitutive heterochromatin contain few genes and therefore may contain a correspondingly low density of *Xist* binding sites.

It has been estimated that there are between 300 and 2000 molecules of *Xist* RNA/nucleus (30). This converts to ~3–20 RNA molecules/Mb of X chromosome DNA (i.e. probably <1/gene) and suggests that individual binding sites most likely influence higher order chromatin structure. *Xist* RNA appears as a large domain comprised of numerous punctate dots at interphase (15,20, this study) which possibly correspond to the individual binding sites mentioned above. Presumably, the banded signal observed at metaphase reflects the concentration of these sites on the condensed chromosome.

Localization of *Xist* RNA on X:autosome rearrangements

Our results with the X:A translocations, Is1Ct and T37H, clearly indicate that *Xist* RNA association and chromosome inactivation occur more efficiently on X chromatin than on the adjacent autosomal material. In a minority of cases, the RNA extends for a short distance into the *cis*-linked autosomal chromatin, with limited autosomal silencing, as indicated by histone H4 hypoacetylation. These data are broadly in line with genetic and cytogenetic studies on X:A translocations (reviewed in ref. 9).

In this study we have analysed X inactivation in cell lines established from adult animals. A key question is whether our observations reflect the situation at the onset of inactivation during early embryogenesis. Specifically, does autosomal material resist the initial spread of inactivation or is there efficient spread and subsequent retreat? The latter hypothesis is supported by classical genetic studies on Is1Ct, which have demonstrated reactivation with ageing of the *albino* (*c*) locus (31,32). More recently, analysis of *Xist* transgenes in interphase nuclei of differentiated ES cells suggests that *Xist* RNA does spread over autosomal material (15,18). Further analysis has revealed that, in two out of three cases, the spread of *Xist* RNA was not maintained in fibroblasts derived from these ES cells (16). These observations support the idea of initial spread followed by retreat of *Xist* RNA, suggesting a failure in maintenance. In contrast, the analysis of a T37H ES cell line (TMA-2) and near-tetraploid EC hybrids ($XXX^4 4^X$) demonstrated no late replication on the chromosome 4 segment of 4^X when either cell line was differentiated *in vitro* (33; N.Takagi, personal communication). In these cases, attenuated spread is detectable immediately after the onset of X inactivation and in a situation where cell selection events are unlikely to play a significant role. This provides compelling evidence that the autosomal material is inherently less sensitive to spreading of the inactivation signal. Taken together these observations suggest that both attenuated spreading and inefficient maintenance contribute to inefficient inactivation of *cis*-linked autosomes.

Although our data demonstrate minimal spread of *Xist* RNA into autosomal material *in cis*, classical genetic studies support inactivation of specific autosomal regions. The *b* locus, located 20 cM from the X:A break point in T37H, is efficiently inactivated (34,35). Interestingly, the *misty* (*m*) locus, located between *b* and the break point, is thought to remain active in T37H, suggesting that the spread of inactivation can be discontinuous (36). In our analysis *Xist* RNA rarely extended as far as the *b* locus but we frequently observed an isolated focus of RNA between the *db* and *b* markers. Binding of *Xist* RNA to this site may be responsible for discontinuous inactivation of *b*. We also observed a region of hypoacetylation between the *db* and *b* markers on some T37H metaphases, but because the antibody to acetylated H4 normally reveals a banded pattern on metaphase chromosomes, we cannot rule out that this region is always hypoacetylated on chromosome 4.

In Is1Ct we found that the inserted region is generally hyperacetylated and free of *Xist* RNA. In a few examples, *Xist* RNA did show limited spread into the autosomal material closest to the translocation boundaries. Limited spreading of *Xist* into autosomal DNA is consistent with reports of variegation of coat colour markers located close to the break points (37). There is, however, evidence for some inactivation of coat colour markers located more centrally in the insertion (38,39). As argued for T37H, this apparent discrepancy may be attributable to discontinuous inactivation effects. It is also possible that there are differences in the extent of inactivation of Is1Ct in fibroblast cell lines compared with adult cells *in vivo*.

A recent study suggests that discontinuous effects may be a common feature of inactivation in X:A rearrangements. Analysis of autosomal gene expression on a human X:A rearrangement indicated that spreading of inactivation was incomplete and non-contiguous (40). Investigations into gene expression status in other X:A translocations will help to reveal the identity of autosomal elements that permit the discontinous spreading of inactivation.

A model for the propagation of X inactivation

Figure 5 illustrates a model, based in part on previous proposals (8,19,41,42), for the role of *Xist* RNA in the spreading of X inactivation. In this model we propose that *Xist* RNA binds to

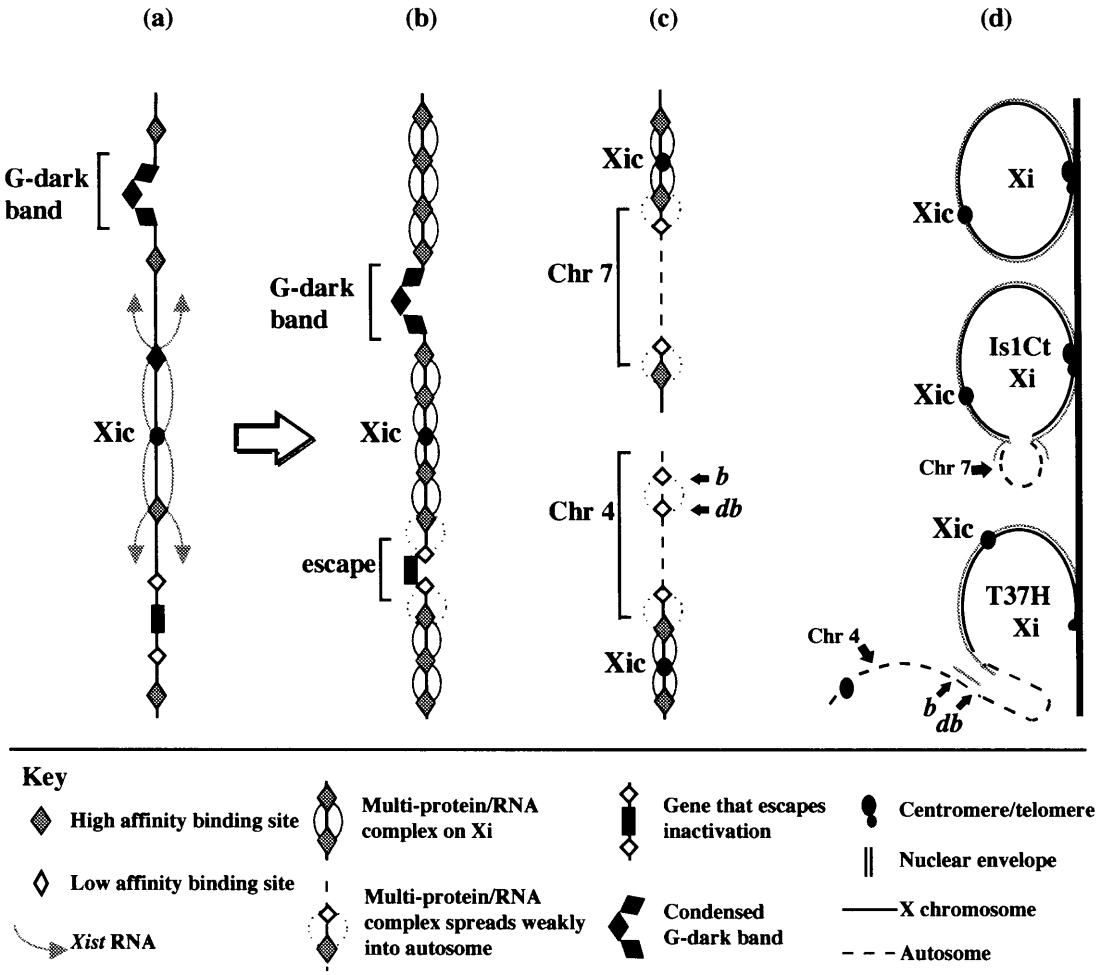

Figure 5. Model for propagation of X inactivation. (**a**) *Xist* RNA binds to high affinity sites close to *Xic*, resulting in a local conformational change, that allows further proteins to bind. Binding sites are absent, inaccessible or less frequent in G-dark bands and in regions that escape inactivation. (**b**) Multiprotein–RNA complexes build up in G-light bands and recruit more distant binding sites by cooperative spreading. G-light bands form condensed heterochromatin and regions that escape 'loop out' from Xi. (**c**) Multiprotein–RNA complexes build up and invade *cis*-linked autosomal material in Is1Ct X (top) and T37H 4^X (bottom). Some autosomal regions, such as that between the *db* and *b* loci on chromosome 4, have *Xist* RNA binding sites allowing local build-up of chromatin condensation complexes. (**d**) Xi condenses to form the Barr body located close to the nuclear periphery in an isolated heterochromatic nuclear compartment. This separates Xi chromatin from the cell transcriptional machinery. Genes that escape inactivation or autosomal material at some distance from Xi chromatin should be free to associate with nuclear transcription complexes. Autosomal regions enriched for *Xist* RNA-binding sites are recruited to the Xi silent domain.

high affinity sites close to the Xic (Fig. 5a) inducing local heterochromatinization which then spreads along the chromosome in a cooperative manner (Fig. 5b). Presumably, there are specific consensus sequences or possibly secondary structures underlying these sites. Binding sites are proposed to be absent or infrequent in gene-poor regions such as constitutive heterochromatin and G-dark bands and in regions where X-linked genes are reported to escape inactivation (Fig. 5a and b).

The failure to inactivate *cis*-linked autosomal chromatin is proposed to stem from the absence, low frequency or low affinity of binding sites. Studies with ectopically integrated *Xist* transgenes indicate that it is possible for certain autosomes to be efficiently inactivated (16). This may indicate either that these autosomes have a higher frequency of *Xist* binding sites or, alternatively, that elevated levels of *Xist* RNA can partially overcome the relative resistance of autosomal chromatin to inactivation. We have observed a limited spread of *Xist* RNA at the X:A boundaries in this study and propose that this is due to a proximity effect in which weak or infrequent autosomal binding sites are unstably recruited into the heterochromatic Xi domain (Fig. 5c). We suggest further that certain autosomal regions, for example the *b* locus in T37H, may respond efficiently to the *Xist* signal due to the presence of high affinity autosomal binding sites (Fig. 5c and d). According to our model, these regions would be recruited into the heterochromatic Xi domain in which chromatin is sequestered from the trancriptional machinery. Intervening regions lacking binding sites would loop out, explaining discontinuous spreading effects such as those thought to occur with *b* and *m* in T37H (36). Similar looping models have recently been put forward to explain PEV effects in *Drosophila* (43,44) and gene silencing by recruitment to centromere clusters in lymphocytes (45).

In summary, we have presented evidence showing that *Xist* RNA preferentially associates with X chromatin *in cis*, supporting the idea of X-specific *Xist* RNA binding elements or 'way stations'. Identifying the nature of *Xist* RNA binding sites and associated proteins presents an important challenge for the future.

MATERIALS AND METHODS

Animals and cell culture

T(X;16)16H/Is1(X;7)Ct double heterozygous females were bred in-house by crossing unbalanced Is1(X;7)Ct/Y males with T(X;16)16H+/+Ta females. The Is1Ct X chromosome is always inactive in these animals. T(X;4)37H females were also bred in-house. Primary lung fibroblast cell lines were generated from 4-week-old female mice by standard methods (46) and were maintained at 37°C, 5% CO_2 in Ham's F12 medium (Gibco) supplemented with 10% fetal calf serum and 50 IU/ml penicillin/streptomycin. Analysis was performed on primary lines derived from two individual animals for each of the translocations. Control XX female (SD1) and XY male (SD2) fibroblasts were derived from standard laboratory strains. Similarly, primary fibroblasts were generated from two common vole species (group *arvalis*) of the genus *Microtus*: *M.rossiaemeridionalis* (found widely distributed throughout Eurasia) and *M.transcaspicus* (endemic to Middle Asia). The animals were trapped in the wild and bred in the Institute of Cytology and Genetics, Novosibirsk, Russia. Rat embryo fibroblasts were a gift from A. Monaco (Wellcome Trust Centre for Human Genetics, Oxford, UK).

Probes for FISH analysis

RNA was detected with DNA probes labelled with biotin by nick translation, while DNA was generally detected with DNA probes similarly labelled with digoxigenin (Dig).

Mouse *Xist* RNA was detected either with GPT16, a 6 kb DNA probe spanning most of exon 1, or with the 35 kb cosmid 11179, which includes the entire *Xist* gene (a gift from L. Herzing, Chester Beatty Laboratories, ICRF, London, UK). Vole *Xist* RNA was detected with both S12 (1.7 kb genomic clone starting 400 bp 5′ of the *Xist* minimal promoter) and RX8 (7 kb probe extending 3′ of S12 to 300 bp in intron 1) together. Vole X chromosome repeats were identified using the 3.3 kb MS3 repeat probe described by Elisaphenko *et al*. (25). Rat *Xist* was detected with a λ clone encompassing the entire *Xist* gene (from A. Monaco).

Autosomal DNA loci on chromosome 4 were identified with the following BAC clones: BAC 54 and BAC 242 mapping to the *diabetes* (*db*) locus (a gift from J. Friedman, Howard Hughes Medical Institute, New York, NY); BAC 286 and BAC 274 mapping to the *brown* (*b*) locus (a gift from I. Jackson, MRC Genetics Unit, Edinburgh, UK). BACs for loci on chromosome 7 were: BAC 194 and BAC 195, isolated using probe *D7HD12* (a gift from G. Kelsey, Queensland Institute of Medical Research, Royal Brisbane Hsopital, Queensland, Australia); BAC 149, isolated using an RT–PCR cDNA product from the mouse *SnrpN* gene (47).

An FITC-conjugated mouse X chromosome paint was obtained from the Cambio STAR*FISH range of paints and a plasmid containing eight copies of mouse centromeric γ-satellite repeat sequences was a gift from N. Dillon (MRC Clinical Sciences Centre, London, UK).

RNA FISH

Fibroblasts were grown on Superfrost Plus glass slides (BDH, Poole, UK) overnight and incubated with ethidium bromide (1.5 µg/ml final concentration) for 2 h before fixation. Cells were swollen with hypotonic solution (75 mM KCl) for 10 min before fixing with 4% (v/v) formaldehyde, 5% (v/v) acetic acid, 0.9% (w/v) NaCl in dH_2O for 20 min at 4°C. Slides were then washed in PBS and stored in 70% ethanol at 4°C until use.

RNA FISH was performed essentially as described by Raap *et al*. (48). Control slides were treated with RNase A, as described below, following the final dehydration step and before probe was applied (data not shown). Approximately 50–100 ng of biotinylated DNA probe, 20 µg yeast tRNA and 5 µg salmon sperm DNA were precipitated together and then dissolved in 10 µl hybridization mix (50% formamide, 2× SSC, 5% dextran sulphate, 300 mM NaCl, 10 mM EDTA, 25 mM NaH_2PO_4, pH 7.4) per slide.

Following hybridization, slides were washed three times for 3 min each in 50% formamide at room temperature, once for 3 min in 50% formamide at 37°C, then once for 3 min in 2× SSC and once for 3 min in 4× SSC, 0.1% Tween-20, both at room temperature. The biotinylated probe was detected with avidin–FITC followed by biotinylated anti-avidin (raised in goat) and a final layer of avidin–FITC. Slides were mounted in Vectashield (Vector Laboratories, Peterborough, UK) antifade containing DAPI counterstain (25 µl/slide). All antibodies were obtained from Vector Laboratories unless otherwise stated.

Slides were examined with an oil immersion ×100 objective on a Leica DMRB fluorescence microscope and selected images were captured with a Photometrics CCD camera coupled to Smartcapture software [Vysis (UK), Richmond, UK].

RNA/DNA FISH

The *Xist* transcript was detected by RNA FISH as described above, the slides were mounted and the coverslips temporarily sealed with Cowgum. Slides were examined under the microscope to check *Xist* RNA signal and selected images were captured to determine whether any signal was lost during further treatment of the slides. Coverslips were then removed in dH_2O and the slides were incubated in RNase A (100 µg/ml) in 2× SSC at 37°C for 1 h before a brief rinse in 2× SSC and dehydration through an ethanol series. The slides were air dried under vacuum and then incubated in 0.7% Triton X-100 (Sigma, St Louis, MO), 0.1 M HCl for 10 min on ice. They were then washed twice in 2× SSC for 5 min at room temperature and denatured in 70% formamide at 75°C for 3–4 min before quenching in ice-cold 70% ethanol for 2 min followed by 2 min each in 90 and 100% ethanol at room temperature and vacuum drying. Approximately 100–200 ng of each Dig-labelled genomic DNA BAC probe, 5 µg salmon sperm DNA and 5 µg mouse COT-1 DNA (Gibco) were precipitated together and dissolved in 10 µl DNA hybridization mix (50% v/v formamide, 2× SSC, 1% v/v Tween-20, 20% v/v dextran sulphate) per slide. The slides were incubated overnight in a humid chamber at 37°C prior to washing in 50% formamide, 50% 2× SSC twice for 5 min each at 45°C, then 0.1× SSC twice for 5 min each at 45°C and finally 4× SSC, 0.1% Tween-20 for 3 min at room temperature.

Dig-labelled DNA probes were detected with rhodamine-conjugated anti-Dig (Boehringer Mannheim, Lewes, UK) and then Texas red-conjugated anti-sheep (TR-AS) as described above. Cells were examined under oil at ×100 for both RNA and DNA signals and selected images were compared with the *Xist* RNA-only results captured previously (data not shown).

Histone H4 acetylation

Fibroblasts were cytospun on to Superfrost Plus glass slides using a cytocentrifuge (Shandon Cytospin, Pittsburgh, PA) as described (26). Antibody 232 against acetylated Lys8 of histone H4 was prepared and characterized as described previously (49–51). Immunolabelling was performed as outlined (26,52) with minor modifications. Following incubation in a humidified chamber with the primary antibody for 1 h at 4°C, slides were washed twice for 5 min in KCM buffer (120 mM KCl, 20 mM NaCl, 10 mM Tris–HCl, pH 8, 0.5 mM EDTA, 0.1% Triton X-100). A biotinylated anti-rabbit antibody was then applied for 1 h at 4°C, the slides again washed in KCM and then fixed for 10 min in ice-cold 3:1 methanol/acetic acid. After fixation, the slides were air dried and stored at –20°C until used *in situ* as described below.

Slides, prepared as described above, were removed from the freezer and allowed to reach room temperature prior to incubation in 2× SSC at 37°C for 30 min. They were then dehydrated through an ethanol series and air dried under vacuum. Cellular DNA was denatured in 70% formamide, 30% 2× SSC for 1 min at 65°C and quenched in ice-cold 70% ethanol for 2 min followed by 2 min each in 90 and 100% ethanol at room temperature and vacuum drying. Dig-labelled DNA BAC probes were denatured and precompeted as described above and the FITC-conjugated X chromosome paint was denatured according to the manufacturer's instructions. DNA probe in 10 µl of hybridization mix was applied to each slide and the slides were incubated overnight at 37°C (see above). After hybridization, the slides were washed twice for 5 min each in 50% formamide at 45°C, twice for 5 min each in 0.1× SSC at 45°C and once for 3 min in 4× SSC, 0.1% Tween-20. The Dig-labelled probes were detected with FITC–AD followed by FITC–AS and the histone H4 antibody 232 was detected with a final layer of streptavidin–TR. The X paint was incubated at 42°C and detected as recommended in the manufacturer's protocol. Slides were mounted and viewed as described above.

ACKNOWLEDGEMENTS

We would like to thank I. Jackson, J. Friedman, N. Dillon and G. Kelsey for providing DNA probes, A. Monaco for the rat *Xist* clones and cell line, N. Takagi for communicating unpublished data and members of the X inactivation group and Mandy Fisher for helpful discussion and criticism of the manuscript. This work was supported by the Medical Research Council, UK.

REFERENCES

1. Lyon, M.F. (1992) Some milestones in the history of X-chromosome inactivation. *Annu. Rev. Genet.*, **26**, 17–28.
2. Rastan, S. and Brown, S.D.M. (1990) The search for the mouse X chromosome inactivation centre. *Genet. Res.*, **56**, 99–106.
3. Barr, M.L. and Carr, D.H. (1961) Correlations between sex chromatin and sex chromosomes. *Acta Cytol.*, **6**, 34–45.
4. Dyer, K.A., Canfield, T.K. and Gartler, S.M. (1989) Molecular cytological differentiation of active from inactive X domains in interphase: implications for X chromosome inactivation. *Cytogenet. Cell Genet.*, **50**, 116–120.
5. Jeppesen, P. and Turner, B.M. (1993) The inactive-X chromosome in female mammals is distinguished by a lack of H4 acteylation, a cytogenetic marker for gene expression. *Cell*, **74**, 281–289.
6. Belyaev, N.D., Keohane, A.M. and Turner, B.M. (1996) Differential underacetylation of histones H2A, H3 and H4 on the inactive X chromosome in human female cells. *Hum. Genet.*, **97**, 573–578.
7. Boggs, B.A., Connors, B., Sobel, R.E., Chinault, A.C. and Allis, C.D. (1996) Reduced levels of histone H3 acetylation on the inactive X chromosome in human females. *Chromosoma*, **105**, 303–309.
8. Riggs, A.D., Singer-Sam, J. and Keith, D.H. (1985) Methylation of the PGK promotor region and an enhancer way-station model for X-chromosome inactivation. In Sandberg, A.A. (ed.), *Biochemistry and Biology of DNA Methylation*. Alan R. Liss, New York, NY, pp. 211–222.
9. Russell, L.B. (1983) X-autosome translocations in the mouse: their characterisation and use as tools to investigate gene inactivation and gene action. In *Cytogenetics of the Mammalian Chromosome*, Part A, *Basic Mechanisms of X Chromosome Behaviour*. Alan R. Liss, New York, NY, pp. 205–250.
10. Russell, L.B. (1961) Genetics of mammalian sex chromosomes. *Science*, **133**, 1795–1803.
11. Brown, C.J., Ballabio, A., Rupert, J.L., Lafreniere, R.G., Grompe, M., Tonlorenzi, R. and Willard, H. (1991) A gene from the region of the human X inactivation centre is expressed exclusively from the inactive X chromosome. *Nature*, **349**, 38–44.
12. Borsani, G., Tonlorenzi, R., Simmler, M.C., Dandolo, L., Arnaud, D., Capra, V., Grompe, M., Pizzuti, A., Muzny, D., Lawrence, C., Willard, H.F., Avner, P. and Ballabio, A. (1991) Characterization of a murine gene expressed from the inactive X chromosome. *Nature*, **351**, 325–328.
13. Brockdorff, N., Ashworth, A., Kay, G.F., Cooper, P., Smith, S., McCabe, V.M., Norris, D.P., Penny, G.D., Patel, D. and Rastan, S. (1991) Conservation of position and exclusive expression of mouse *Xist* from the inactive X chromosome. *Nature*, **351**, 329–331.
14. Penny, G.D., Kay, G.F., Sheardown, S.A., Rastan, S. and Brockdorff, N. (1996) Requirement for *Xist* in X chromosome inactivation. *Nature*, **379**, 131–137.
15. Lee, J.T., Strauss, W.M., Dausman, J.A. and Jaenisch, R. (1996) A 450 kb transgene displays properties of the mammalian X-inactivation center. *Cell*, **86**, 83–94.
16. Lee, J.T. and Jaenisch, R. (1997) Long-range *cis* effects of ectopic X-inactivation centres on a mouse autosome. *Nature*, **386**, 275–279.
17. Marahrens, Y., Panning, B., Dausman, J., Strauss, W. and Jaenisch, R. (1997) *Xist* deficient mice are defective in dosage compensation but not spermatogenesis. *Genes Dev.*, **11**, 156–166.
18. Herzing, L.B.K., Romer, J.T., Horn, J.M. and Ashworth, A. (1997) *Xist* has properties of the X-chromosome inactivation centre. *Nature*, **386**, 272–275.
19. Brown, C.J., Hendrich, B.D., Rupert, J.L., Lafreniere, R.G., Xing, Y., Lawrence, J. and Willard, H.F. (1992) The human *XIST* gene: analysis of a 17 kb inactive X specific RNA that contains conserved repeats and is highly localised within the nucleus. *Cell*, **71**, 527–542.
20. Clemson, C.M., McNeil, J.A., Willard, H.F. and Lawrence, J.B. (1996) *XIST* RNA paints the inactive X chromosome at interphase: evidence for a novel RNA involved in nuclear/chromosome structure. *J. Cell. Biol.*, **132**, 259–275.
21. Zakian, S.M., Nesterova, T.B., Cheryaukene, O.V. and Bochkarev, M.N. (1991) Heterochromatin as a factor affecting X-inactivation in interspecific female vole hybrids (Microtidae, Rodentia). *Genet. Res. Camb.*, **58**, 105–110.
22. Mazurok, N.A., Nesterova, T.B. and Zakian, S.M. (1995) High-resolution G-banding of chromosomes in *Microtus subarvalis* (Rodentia, Arvicolidae). *Hereditas*, **123**, 47–52.
23. Mazurok, N.A., Rubtsova, N.V., Isaenko, A.A., Nesterova, T.B. and Zakian, S.M. (1996) Comparative analysis of chromosomes in *Microtus transcaspicus* and *Microtus subarvalis* (Arvicolidae, Rodentia): high-resolution G-banding and localization of NORs. *Hereditas*, **124**, 243–250.
24. Nesterova, T.B., Duthie, S.M., Mazurok, N.A., Isaenko, A.A., Rubtsova, N.V., Zakian, S.M. and Brockdorff, N. (1998) Comparative mapping of X chromosomes in vole species of the genus *Microtus*. *Chromosome Res.*, **6**, 41–48.
25. Elisaphenko, E.A., Nesterova, T.B., Duthie, S.M., Ruldugina, O.V., Rogozin, I.B., Brockdorff, N. and Zakian, S.M. (1998) Repetitive DNA sequences in the common vole: cloning, characterisation and chromosome localisation of two novel complex repeats MS3 and MS4 from the genome of the East-European vole *Microtus rossiaemeridionalis*. *Chromosome Res.*, **6**, in press.
26. Keohane, A.M., O'Neill, L.P., Belyaev, N.D., Lavender, J.S. and Turner, B.M. (1996) X-inactivation and histone H4 acetylation in embryonic stem cells. *Dev. Biol.*, **180**, 618–630.
27. Wakefield, M.J., Keohane, A.M., Turner, B.M. and Graves, J.A. (1997) Histone underacetylation is an ancient component of mammalian X chromosome inactivation. *Proc. Natl Acad. Sci. USA*, **94**, 9665–9668.
28. Russell, L.B. and Cacheiro, N.A. (1978) The use of mouse X–autosome translocations in the study of X-inactivation patterns and non-randomness. In Russell, L.B. (ed.), *Genetic Mosaics and Chimeras in Mammals*. Plenum Press, New York, NY, pp. 393–416.
29. Panning, B. and Jaenisch, R. (1998) RNA and the epigenetic regulation of X chromosome inactivation. *Cell*, **93**, 305–308.

30. Buzin, C.H., Mann, J.R. and Singer-Sam, J. (1994) Quantitative RT-PCR assays show *Xist* RNA levels are low in mouse female adult tissue, embryos and embryoid bodies. *Development*, **120**, 3529–3536.
31. Cattanach, B.M. and Isaacson, J.H. (1965) Genetic control over the inactivation of autosomal genes attached to the X-chromosome. *Z. Vererbungslehre*, **96**, 313–323.
32. Cattanach, B.M., Pollard, C.E. and Perez, J.N. (1969) Controlling elements in the mouse X-chromosome. I. Interaction with the X-linked genes. *Genet. Res. Camb*., **37**, 151–160.
33. Takagi, N. (1993) Variable X chromosome inactivation patterns in near-tetraploid murine EC × somatic cell hybrid cells differentiated *in vitro*. *Genetica*, **88**, 107–117.
34. Beechey, C.V. and Searle, A.G. (1977) *Mouse Newslett*., **56**, 39.
35. Searle, A.G. and Beechey, C.V. (1977) *Mouse Newslett*., **57**, 18.
36. Searle, A.G., Beechey, C.V., Evans, E.P. and Kirk, M. (1983) Two new X-autosome translocations in the mouse. *Cytogenet. Cell Genet*., **3**, 279–292.
37. Cattanach, B.M. (1970) Controlling elements in the mouse X-chromosome. III. Influence upon both parts of an X divided by rearrangement. *Genet. Res. Camb*., **16**, 293–301.
38. Cattanach, B.M. (1961) A chemically-induced variegated-type position effect in the mouse. *Z. Vererbungslehre*, **92**, 165–182.
39. Russell, L.B. and Montgomery, C.S. (1965) The use of X-autosome translocations in locating the X-chromosome inactivation centre. *Genetics*, **52**, 470–471.
40. White, W.M., Willard, H.F., Van Dyke, D.L. and Wolff, D.J. (1998) The spreading of X inactivation into autosomal material of an X;autosome translocation: evidence for a difference between autosomal and X-chromosomal DNA. *Am. J. Hum. Genet*., **63**, 20–28.
41. Brockdorff, N., Ashworth, A., Kay, G.F., McCabe, V.M., Norris, D.P., Cooper, P.J., Swift, S. and Rastan, S. (1992) The product of the mouse *Xist* gene is a 15kb inactive X specific transcript containing no conserved ORF and located in the nucleus. *Cell*, **71**, 515–526.
42. Brockdorff, N. (1997) Convergent themes in X chromosome inactivation and autosomal imprinting. In Reik, W. and Surani, A. (eds), *Genomic Imprinting, Frontiers in Molecular Biology Series*. Oxford University Press, Oxford, UK, pp. 191–210.
43. Csink, A.K. and Henikoff, S. (1996) Genetic modifications of heterochromatic associations and nuclear organization in *Drosophila*. *Nature*, **381**, 529–531.
44. Dernburg, A.F., Broman, K.W. Fung, J.C., Marshall, W.F., Philips, J., Agard, D.A. and Sedat, J.W. (1996) Perturbation of nuclear architecture by long-distance chromosome interactions. *Cell*, **85**, 745–759.
45. Brown, K.E., Guest, S.S., Smale, S.T., Hahm, K., Merkenschlager, M. and Fisher, A.G. (1997) Association of transcriptionally silent genes with Ikaros complexes at centromeric heterochromatin. *Cell*, **91**, 845–854.
46. Nesterova, T.B., Mazurok, N.A., Matveeva, N.M., Shilov, A.G., Yantsen, E.I., Ginsburg, E.K., Goss, S.J. and Zakian, S.M. (1994) Demonstration of the X-linkage and order of the genes *GALA*, *G6PD*, *HPRT* and *PGK* in two vole species of the genus *Microtus*. *Cytogenet. Cell Genet*., **65**, 250–255.
47. Ozcelik, T., Leff, S., Robinson, W., Donlon, T., Lalande, M., Sanjines, E., Schinzel, A. and Francke, U. (1992) Small nuclear ribonucleoprotein polypeptide N (SNRPN), an expressed gene in the Prader–Willi syndrome critical region. *Nature Genet*., **2**, 265–269.
48. Raap, A.K., Van de Rijke, F.M., Dirks, R.W., Sol, C.J., Boom, R. and Van der Ploeg, M. (1991) Bicolor fluorescence *in situ* hybridisation to intron and exon mRNA sequences. *Exp. Cell Res*., **197**, 319–322.
49. Turner, B.M. and Fellows, G. (1989) Specific antibodies reveal ordered and cell-cycle-related use of histone H4 acetylation sites in mammalian cells. *Eur. J. Biochem*., **79**, 131–139.
50. Turner, B.M., O'Neill, L.P. and Allan, I.M. (1989) Histone H4 acetylation in human cells. Frequency of acetylation at different sites defined by immunolabelling with site-specific antibodies. *FEBS Lett*., **253**, 141–145.
51. Turner, B.M., Birley, A.J. and Lavender, J. (1992) Histone H4 isoforms acetylated at specific lysine residues define individual chromosomes and chromatin domains in *Drosophila* polytene nuclei. *Cell*, **69**, 375–384.
52. Jeppesen, P., Mitchell, A., Turner, B.M. and Perry, P. (1992) Antibodies to defined histone epitopes reveal variations in chromatin conformation and underacetylation of centromeric heterochromatin in human metaphase chromosomes. *Chromosoma*, **101**, 322–332.